Available online at www.sciencedirect.com
ScienceDirect
Journal of Solid State Chemistry 180 (2007) 1575–1581
JOURNAL OF SOLID STATE CHEMISTRY
www.elsevier.com/locate/jssc

Synthesis, structure and electronic structure of a new polymorph of $CaGe_2$

Paul H. Tobash, Svilen Bobev*

Department of Chemistry and Biochemistry, University of Delaware, Newark, Delaware 19716, USA

Received 31 January 2007; received in revised form 1 March 2007; accepted 5 March 2007
Available online 12 March 2007

Abstract

Reported are the flux synthesis, the crystal structure determination, the properties and the band structure calculations of a new polymorph of $CaGe_2$, which crystallizes with the hexagonal space group $P6_3mc$ (no. 186) with cell parameters of $a = 3.9966(9)$ and $c = 10.211(4)$ Å ($Z = 2$; Pearson's code $hP6$). The structure can be viewed as puckered layers of three-bonded germanium atoms, $^2_\infty[Ge_2]^{2-}$, which are stacked along the direction of the c-axis in an $ABAB$-fashion. The germanium polyanionic layers are separated by the Ca cations. As such, this structure is closely related to the structure of the other $CaGe_2$ polymorph, which crystallizes with the rhombohedral $CaSi_2$ type in the $R\bar{3}m$ space group (No. 166), where the $^2_\infty[Ge_2]^{2-}$ layers are arranged in an $AA'BB'CC'$-fashion, and are also interspaced by Ca^{2+} cations. LMTO calculations suggest that in spite of the formal closed-shell configuration for all atoms and the apparent adherence to the Zintl rules for electron counting, i.e., $Ca^{2+}[3b\text{-}Ge^{1-}]_2$), the phase will be a poor metal due to a small Ca-3d–Ge-4p band overlap. Magnetic susceptibility measurements as a function of the temperature indicate that the new $CaGe_2$ polymorph exhibits weak, temperature independent, Pauli-paramagnetism.

Keywords: Crystal structure; $CaGe_2$; Zintl phase; Flux growth; Polymorph

1. Introduction

The silicides and germanides of the alkaline-earth metals (AE hereafter) have received increased attention in recent years due to their unique crystal chemistry and physical properties [1]. The structures of these compounds can range from simple close packing of atoms, through small metal clusters and layered arrangements to three-dimensional networks. Polytypism and polymorphism are also a reoccurring theme here—take for example the three polymorphic forms of $BaSi_2$: trigonal ($P\bar{3}m1$) [2a], orthorhombic ($Pnma$) [2b], and cubic ($P4_132$) [2a], respectively, all featuring completely different bonding arrangements. Of course, there are many other examples where interesting and unusual properties abound, such as the superconductivity in $CaSi_2$ [1a] and Ba_6Ge_{25} [1f], the unexpected metallicity in the salt-like Ca_5Ge_3 phase [1b], etc. The appeal of these intermetallic compounds was further fueled by the invention of processes that use them as precursors in the syntheses of a variety of nano-structured materials [3].

Our interest in these systems came from a different perspective, and mainly originated from the successful use of Mg and Ca in particular to replace lanthanide elements in the structures of $RE_{5-x}Mg_xGe_4$ and $RE_{5-x}Ca_xGe_4$ (RE = rare-earth metals) [4]. Such substitutions of magnetic with non-magnetic metal atoms create opportunities for fine-tuning the magnetic properties. Motivated by that and by the success in applying the flux-growth methods towards the synthesis of new binary and ternary phases, which are inaccessible by other synthetic routes [5], we undertook systematic studies of the phase equilibria in the AE–In–Ge and RE–In–Ge systems. These were initiated after the discovery of the RE_2InGe_2 family (RE = Sm, Gd–Ho, Yb) [6], for which magnetic susceptibility measurements confirm localized-moment magnetism typical for the free RE^{3+} ions [7]. The only exception of that series is Yb_2InGe_2, which exhibits a temperature independent paramagnetism, consistent with a closed-shell f^{14} configuration, i.e., Yb^{2+}. This, and the very similar crystal

*Corresponding author. Fax: +1 302 831 6335.
E-mail address: bobev@udel.edu (S. Bobev).

0022-4596/$ - see front matter © 2007 Elsevier Inc. All rights reserved.
doi:10.1016/j.jssc.2007.03.003

chemistry of Yb and Ca, inspired us to seek after the isoelectronic Ca_2InGe_2. Instead, the conducted In-flux reactions afforded the formation of a new binary phase $CaGe_2$, which is denoted hereafter as α-$CaGe_2$. This compound is a polymorph of the well-known $CaGe_2$ (β-$CaGe_2$ hereafter), crystallizing with the rhombohedral $CaSi_2$ type [8].

The discovery of polymorphism in the Ca–Ge system is rather surprising since it is not indicated neither in the original binary phase diagram [9] nor in its recent revision [10]. These two studies suggest only one thermodynamically stable $CaGe_2$ compound, β-$CaGe_2$ (sometimes denoted as "tr6 phase"). A survey of the literature showed that the existence of a second modification of $CaGe_2$ (referred to as "h2 phase") has been mentioned in a previous work on epitaxially grown thin films [11]. Nevertheless, to date, the crystal structure and the bulk synthesis and properties of this phase are not established. Herein, we report the synthesis of α-$CaGe_2$ as large, well-defined single crystals, and its structure determination from single-crystal and powder X-ray diffraction. Since the structure of the β-$CaGe_2$ polymorph has been known for more than 6 decades, but never refined, we also report the refined from single-crystal X-ray diffraction data atomic positions and thermal parameters for β-$CaGe_2$. The similarities and the differences between the two polymorphs are discussed in the context of the structural studies; band structure calculations and susceptibility measurements for the newly discovered α-$CaGe_2$ are presented as well.

2. Experimental

2.1. Synthesis

All manipulations were performed inside an argon-filled glove box with controlled oxygen and moisture levels below 1 ppm or under vacuum. The starting materials were stored in a glove box and used as received: Ca (with purity >99.9%, Aldrich), Ge (lump, 99.999%, Acros) and In (shot, 99.99%, Alfa-Aesar). The reactions were carried out by loading a mixture of the elements in a ratio of Ca:Ge:In = 1:1:10 in alumina crucibles, and subsequently enclosing them in evacuated fused silica ampoules. The following temperature profile was employed: (1) heating to 1233 K at a rate of 200°/h; (2) homogenization at 1233 K for 25 h; and (3) slow cooling to 873 K at a rate of 10°/h. At this point, the ampoules were quickly removed and the In was separated from the reaction product through centrifugation. Further details on In-flux growth techniques can be found elsewhere [6]. The typical outcomes of such reactions were large but irregular-shaped crystals, with dark to black color and metallic luster. They showed signs of oxidation after a few hours in air.

Attempts to synthesize the hexagonal α-$CaGe_2$ polymorph by stoichiometric reactions in sealed Nb tubes failed. For these experiments, mixtures of Ca and Ge in a ratio of 1:2 were heated quickly above the melting point of Ge (1211 K), reacted overnight and allowed to cool to room temperature. Instead of α-$CaGe_2$, the product of such reactions was the rhombohedral β-$CaGe_2$ form [8], and small amounts of CaGe [8] and elemental Ge as side products. The crystals of β-$CaGe_2$ had similar appearance to those of α-$CaGe_2$, i.e., they were black, brittle and sensitive to air and moisture.

The possibility to synthesize new polymorphs of Sr and Ba digermanides, isostructural with α-$CaGe_2$ was also explored but proved unsuccessful. The In-flux reactions of the heaviest AE elements and germanium yielded the orthorhombic $SrGe_2$ (*Pnma*) [8] and tetragonal $BaIn_4$ (*I*4/*mmm*), respectively [8]. Attempts to prepare analogous compounds of Eu and Yb were also made but led to the growth of very large crystals of $EuGe_2$ [12] and Yb_3Ge_5 [13], respectively.

2.2. Powder X-ray diffraction

X-ray powder diffraction patterns were taken at room temperature on a Rigaku Miniflex powder diffractometer using monochromatized Cu$K\alpha$ radiation. To allow for handling the air-sensitive α-$CaGe_2$ and β-$CaGe_2$, the table-top diffractometer was enclosed in a glove-box. Typical runs included θ–θ scans ($2\theta_{max} = 80°$) with scan-steps of 0.05° and 5 s counting time per step. Data analysis was carried out using the JADE 6.5 software package. Samples were prepared by grinding the shiny and irregular morphologies to a fine powder. For both polymorphs the intensities and the positions of the experimentally observed peaks matched very well with those calculated from the refined crystal structures. Graphical representation of the experimental and the simulated powder patterns, along with tabulated intensities and *h k l* indices are provided as supplementary material (see Appendix A).

2.3. Single-crystal X-ray diffraction

Crystals from both α-$CaGe_2$ and β-$CaGe_2$ were chosen in the glove-box, mounted on glass fibers (using Paratone N oil) and quickly placed on the gonoimeter of a Bruker SMART CCD-based diffractometer. The measurements were carried out at 120(2) K (by cooling with a cold nitrogen stream), which also helped protecting the crystals from decomposition. For both compounds, full spheres of diffraction data were collected in four batch runs at different ω and ϕ angles. Frame width was 0.4° in ω and because the crystals diffracted very strongly, the data acquisition rate was 8 s/frame. The data collection, data integration, and cell refinement were carried out using the SMART and SAINT programs, respectively [14]. SADABS was used for semi-empirical absorption correction based on equivalents [15]. The structures were solved by direct methods and refined by full matrix least-squares methods on F^2 using the SHELX-package [16]. All sites were refined with anisotropic displacement parameters and full occupancies. The refinements showed no indications

Table 1
Selected single crystal data and structure refinement parameters for both $CaGe_2$ polymorphs

Empirical formula	$CaGe_2$	
Formula weight	185.26 g/mol	
Collection temperature	120(2) K	
Radiation, wavelength (λ)	Mo$K\alpha$, 0.71073 Å	
Crystal system	Hexagonal (α-form)	Rhombohedral (β-form)
Space group	$P6_3mc$	$R\bar{3}m$
Unit cell dimensions	$a = 3.9966(9)$ Å	$a = 3.9872(9)$ Å
	$c = 10.211(4)$ Å	$c = 30.583(8)$ Å
Unit cell volume, Z	141.24(7) Å^3, 2	421.06(17) Å^3, 6
Density (ρ_{calc})	4.36 g/cm^3	4.38 g/cm^3
Absorption coefficient (μ)	22.73 mm^{-1}	22.87 mm^{-1}
Crystal size	0.04 × 0.04 × 0.03 mm^3	0.08 × 0.06 × 0.05 mm^3
Reflections collected, R_{int}	1322, 0.0327	1553, 0.0263
Unique reflections	141	156
Data/restrains/parameters	131/1/11	137/0/10
GOF on F^2	1.124	1.076
Absolute structure parameter	0.11(3)	N/a
Final R indices[a] ($I > 2\sigma_{(I)}$)	$R_1 = 0.0113$	$R_1 = 0.0143$
	w$R_2 = 0.0275$	w$R_2 = 0.0327$
Final R indices[a] (all data)	$R_1 = 0.0143$	$R_1 = 0.0170$
	w$R_2 = 0.0283$	w$R_2 = 0.0338$

[a] $R_1 = \Sigma||F_o|-|F_c||/\Sigma|F_o|$; $wR_2 = [\Sigma[w(F_o^2-F_c^2)^2]/\Sigma[w(F_o^2)^2]]^{1/2}$, and $w = 1/[\sigma^2F_o^2+(AP)^2+BP]$, $P = (F_o^2+2F_c^2)/3$; A and B, weight coefficients.

Table 2
Atomic coordinates and equivalent isotropic displacement parameters (U_{eq} [a]) for α- and β-$CaGe_2$

Atom	Wyckoff position	x	y	z	U_{eq} (Å^2)
α–$CaGe_2$					
Ca	2b	1/3	2/3	0.2927(2)	0.0087(4)
Ge1	2a	1/3	2/3	0.60431(3)	0.0086(2)
Ge2	2b	0	0	0.0000(1)	0.0070(2)
β–$CaGe_2$					
Ca	6c	0	0	0.08099(3)	0.0093(3)
Ge1	6c	0	0	0.18465(2)	0.0074(2)
Ge2	6c	0	0	0.35007(2)	0.0089(2)

[a] U_{eq} is defined as one third of the trace of the orthogonalized U^{ij} tensor.

that any site could be partially occupied or mixed with another element—when freed to vary the site occupancies did not deviate more than 3σ from full. Further details of the data collection and structure refinement parameters are given in Table 1. The final positional and equivalent displacement parameters and important bond distances for both α- and β-$CaGe_2$ are provided in Tables 2 and 3, respectively [17]. Additional discussion on the structure refinements is provided as supplementary information (see Appendix A).

2.4. Electronic structure calculations

The band structure calculations were performed using the LMTO-47 package [18], which is based on the tight-binding linear-muffin-tin orbital (LMTO) method in the local density (LDA) and atomic sphere (ASA) approximations [19]. Reciprocal space integrations are calculated by the tetrahedron method [20]. The crystal orbital Hamilton population (COHP) method is used for the analysis of bonding interactions [21], analogous to the crystal orbital overlap population (COOP) method used in the semiempirical Hückel calculations [22]. The Fermi level is set to zero; the COHP diagram is drawn by reversing it with respect to the energy scale (i.e., –COHP vs. E). This is done so that the calculated peak values are negative for antibonding and positive for bonding interactions. The chosen basis set contained the 4s, 4p, and 3d orbitals for both the Ca and Ge atoms. A total of 72 irreducible k-points were used in the Brillouin zone.

Table 3
Selected interatomic distances in α- and β-$CaGe_2$

α-$CaGe_2$			β-$CaGe_2$		
Atom pair		Distance (Å)	Atom pair		Distance (Å)
Ge1–	Ge2 × 3	2.5414(7)	Ge1–	Ge1 × 3	2.5513(7)
	Ca × 3	3.0041(14)		Ca × 3	3.0960(9)
	Ca	3.182(2)		Ca	
Ge2–	Ge1 × 3	2.5414(7)	Ge2–	Ge2 × 3	2.5194(7)
	Ca × 3	3.131(2)		Ca × 3	3.0268(9)
Ca–	Ge1 × 3	3.0041(14)	Ca–	Ge2 × 3	3.0268(9)
Ca–	Ge2 × 3	3.131(2)	Ca–	Ge1 × 3	3.0960(9)
Ca–	Ge1	3.182(2)	Ca–	Ge1	3.1701(13)

2.5. Magnetic susceptibility measurements

Field-cooled and zero-field cooled dc magnetization (M) measurements were performed for the title compound using a Quantum Design MPMS SQUID magnetometer. The measurements were completed in the temperature range from 10 to 300 K and in an applied magnetic field (H) of 500 Oe. For these measurements, the sample was secured in a custom-designed sample holder for air-sensitive materials [23]. The raw magnetization data were corrected for the holder contribution and converted to molar susceptibility (χ_m). The susceptibility in the temperature range from room temperature to 10 K varied between ca. 3–10 × 10^{-4} emu/mol, and the small increase in the χ_m value with decreasing the temperature is most certainly due to a small paramagnetic impurity. No indication of superconductivity was observed in the measured temperature interval. A plot of the temperature dependence of the magnetic susceptibility is provided as supplementary material (see Appendix A).

3. Results and discussion

3.1. Structure and bonding

α-$CaGe_2$ crystallizes with the hexagonal space group $P6_3mc$ (No. 186) and its structure contains one calcium and

two germanium atoms in the asymmetric unit, all three in special positions (Table 2). The structure can be readily described as being made up of six-membered rings of Ge atoms that are fused together to form infinite layers and Ca atoms enclosed between them, as shown in Fig. 1. The topology of the Ge-layers can be derived from that of the graphite-like hexagonal nets by slight puckering. These layers are stacked along the direction of the hexagonal *c*-axis in a way that they are not eclipsed, but rather staggered. Such bonding patterns are a common motif in the crystal chemistry of many intermetallic phases, not only for silicides or germanides [8].

The structure of the hexagonal α-$CaGe_2$ polymorph is closely related to the structure of the long-known rhombohedral β-$CaGe_2$ form, and it is worthwhile comparing them side-by-side (Fig. 1). At a first glance, both structures look very much alike since the puckered layers of 3-bonded Ge atoms are a common thread. However, one notices a subtle difference in the way these layers are stacked along the crystallographic *c*-axis in both structures. In the case of α-$CaGe_2$, the stacking scheme can be envisioned as an *ABAB*-like array, commonly found in many hexagonally closed-packed structures [8]. In the structure of β-$CaGe_2$ on the other hand, due to the very long *c*-axis (>30 Å, Table 1), a more complex stacking sequence is observed. The ordering of the layers here can be described as an $AA'BB'CC'$-like array, i.e., a stacking pattern, which repeats every six layers, and where the layers of the same kind are shifted by $\frac{2}{3}\vec{a}$ and $\frac{1}{3}\vec{b}$ with respect to each other.

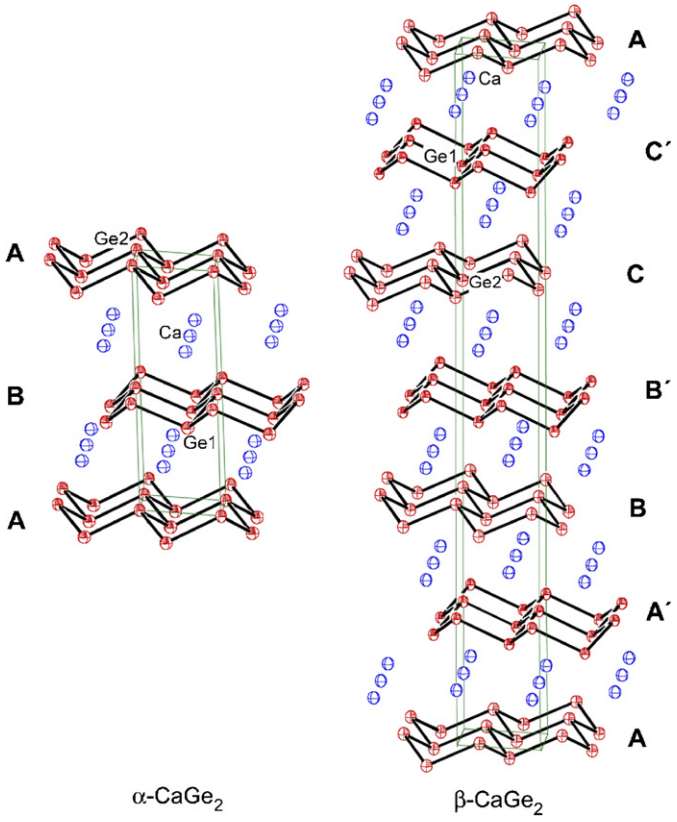

Fig. 1. Projections of the crystal structures of α-$CaGe_2$ and β-$CaGe_2$ viewed approximately down the *a*-axis. Thermal ellipsoids in both cases are drawn at the 95% probability level and the unit cells are outlined. Online color code: Ca atoms are drawn as blue crossed ellipsoids and Ge atoms as red full ellipsoids.

Ge–Ge contacts for both forms of $CaGe_2$ are very similar and range from ca. 2.52 to ca. 2.55 Å (Table 3). These are slightly longer than the Ge–Ge distances in elemental Ge [24] due to the partially reduced formal oxidation state of Ge, and compare well with the Ge–Ge distances in other AE germanides [1b,25]. One important difference however should be explicitly noted: despite having two crystallographic sites for the Ge atoms, α-$CaGe_2$ has only one kind of Ge–Ge bond with a distance that measures 2.5414(7) Å. In contrast, the β-phase has two types of Ge–Ge distances measuring 2.5513(7) Å for the Ge1–Ge1 within the $A'B'C'$ layers, and 2.5194(7) Å for the Ge2–Ge2 pairs within *ABC* layers, respectively (Table 3). In that regard, the layers in the hexagonal α-$CaGe_2$ can be considered as an intermediate between the two different layers in the rhombohedral β-$CaGe_2$.

The coordination of the Ca atoms in both structures is very similar too. Fig. 2 illustrates that the seven-coordinate Ca atom in both structures is located near the center of a distorted trigonal prism with one of its triangular faces capped. However, because of the above-mentioned systematic differences between the germanium layers in α- and β-$CaGe_2$, it can be expected that the coordination polyhedra of the Ca cations in both structures will differ in a subtle way. Each Ca atom in α-$CaGe_2$ is surrounded by 3 next-nearest Ge1 neighbors (at 3.004 Å), and three Ge2 neighbors a bit further away, 3.131 Å. The seventh neighbor, Ge1 is at a distance 3.182 Å (Table 3). The average Ca–Ge distance in this structure is 3.084 Å and it is in good agreement with those found in other Ca–Ge binaries, Ca_5Ge_3 [1b], and CaGe [8], to name a few. The distances in β-$CaGe_2$ are very similar, although the range is somewhat narrower—from 3.027 to 3.170 Å (Table 3), and

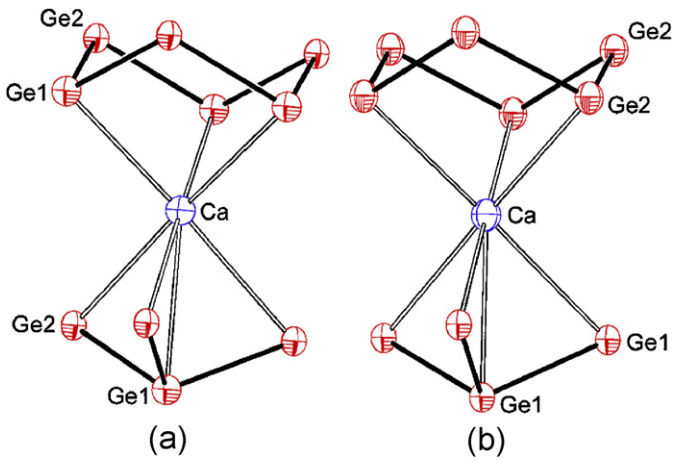

Fig. 2. Coordination polyhedra of the Ca cations for α-$CaGe_2$ (a) and β-$CaGe_2$ (b). Relevant bond distances are listed in Table 3. Online color: same as in Fig. 1.

the average Ca–Ge distance is slightly smaller, 3.077 Å. This indicates that the Ca cations are positioned closer to the geometric center of the coordination polyhedron and are more tightly coordinated in β-$CaGe_2$ than they are in α-$CaGe_2$.

Lastly, it is instructive to mention the ease of synthesis of a second polymorph of $CaGe_2$ within the context of the state-of-the-art knowledge on the Ca–Ge phase diagram [9]. After all, it was revisited recently and a new compound near the equiatomic composition was discovered [10]. Neither version of the phase diagram provides any indication that another form of the congruently melting $CaGe_2$ can exist. The same holds true for the Ca–Si diagram, even though structural studies have identified two more $CaSi_2$ polymorphs, a rhombohedral one (with *ABC*-stacked layers) and a body-centered tetragonal one (with framework of the α-$ThSi_2$ type) [26].

Our own studies of the Ge-rich part of the Ca–Ge phase diagram and attempts to make α-$CaGe_2$ from stoichiometric reactions in sealed tubes suggest that there is only one stable compound, β-$CaGe_2$. However, the same reactions carried out in In flux, almost invariably with the temperature, produce pure phase α-$CaGe_2$. This could suggest that the latter is not a true binary phase but rather a ternary $CaGe_{2-x}In_x$ compound; however, there are several experimental results that rule out such a hypothesis. First, α-$CaGe_2$ can be made from pure Ca and Ge as epitaxially grown thin films [11] with unit cell parameters that match well with those we report for the In-flux grown crystals; second—the structure refinements from single-crystal data unequivocally show that all Ge occupancies are full, and α-$CaGe_2$ is a line compound. Therefore, the above mentioned differences in the synthesis of the both polymorphs are an indication that the faster diffusion and more facile conditions for crystal growth in molten In favor the formation of the faster growing but metastable nuclei (i.e., α-$CaGe_2$), whereas all classic high-temperature syntheses (e.g. direct fusion of pure elements) result in the formation of the thermodynamically more stable phase (i.e., β-$CaGe_2$). Similar polymorphism and dependence on the synthetic conditions were recently discovered within the RE_3Ge_5 family (*RE* = Sm, Gd, Dy) [27] and the $RENiGe_2$ family (*RE* = Dy, Ho, Er, Tm, Yb, Lu) [28], where the "kinetic" products can be synthesized by the flux method only; on the other hand, the thermodynamically stable products are accessible by different solid-state routes.

3.2. Electron count and band structure

The nature of cation–anion interactions in AE and rare-earth germanides and silicides has been the subject of many experimental and theoretical studies [1a–b,12,29]. It is well established that if the covalency in such interactions is completely abandoned, rationalization of the structure and the bonding can be derived from the simplified, yet useful Zintl–Klemm formalism [30]. An effortless account of the $CaGe_2$ structure can be made using this approach—by assuming an electron transfer from the more electropositive Ca to the more electronegative Ge and assigning a formal charge of "1–" to the latter (three-bonded germanium needs an additional electron to achieve a filled valence shell), the formula can be broken down to $Ca^{2+}[3b\text{-}Ge^{1-}]_2$. This means that formally, the compound should be completely charge-balanced, as the typical ionic salts or semiconductors. However, the temperature independent Pauli-like paramagnetism (above) suggests that $CaGe_2$ exhibits metallic behavior, corroborated by the electronic structure calculations. This "shortcoming" of the Zintl concept is well-known and a recent and very detailed case study on Ca_5Ge_3 and related compounds demonstrates that the overestimated electron transfer and mixing of cation–anion states accounts for the "violations" of the Zintl rules [1b].

To verify that this is the case here and to further examine the bonding in α-$CaGe_2$, its band structure was calculated using the LMTO-ASA method. Fig. 3 shows a plot of the band structure, the projected density of states (DOS) and the COHP, all drawn on the same scale. As can be seen

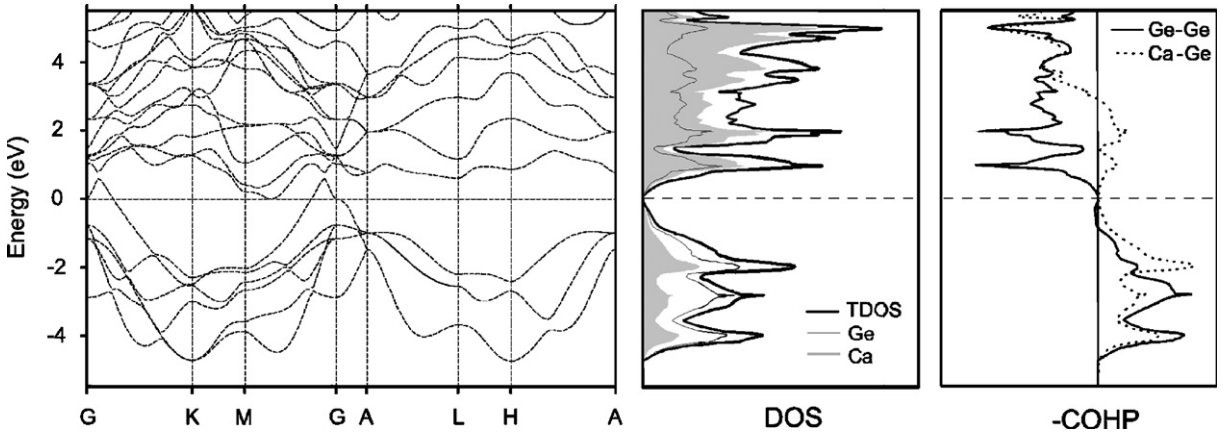

Fig. 3. The band structure (left), total density of states (center), and integrated—COHP (right) for α-$CaGe_2$. The total DOS is drawn with a bold black line, the partial DOS for Ge is drawn with a light gray line, and Ca DOS is shown as the shaded area. The corresponding COHP for the Ge–Ge and Ca–Ge interactions are shown with solid and dashed lines, respectively.

from the figure, a sizeable gap exists at the Fermi level, where the *d* states of Ca and *p* states of Ge are clearly dominating the region near it. The COHP diagram indicates that the Ge–Ge interactions are very much "optimized", while there is a slight electron deficiency of the Ca–Ge interactions. Undoubtedly, the Ge–Ge bonding "controls" the structure and the very small antibonding portion from the Ge–Ge COHP curves may be attributed to π^*-interactions between the two adjacent layers along the *c*-axis, similar to the bonding picture in the related $EuGe_2$ [12]. A hypothetical hexagonal structure of $CaSi_2$ (isostructural with $EuGe_2$) has also been found to have relatively close band-structure characteristics [29a].

However, one must note that there are a few bands (most notably around the G-point) that cut through the band gap. These dispersed bands, mainly originating from *d*-orbitals on Ca are the principal reason for the poorly metallic behavior of α-$CaGe_2$. Such result is in accordance with the recent analyses of the bonding and the electronic structure of $EuGe_2$ [12] and Ca_5Ge_3 [1b], both being examples of metallic Zintl phases. These findings are also supported by the band calculations on the rhombohedral $CaSi_2$ phase, which as discussed already is isostructural with β-$CaGe_2$. Similar to the band structure of $CaGe_2$, the $CaSi_2$ one also has dispersed Si-*p* and Ca-*d* states, which are again mixed near the Fermi level and explain its metallic character [29a–b]. The different stacking arrangements and their effects on the electronic structure of $CaSi_2$ ($R\bar{3}m$) have also been studied and suggest that the partial DOS for the two crystallographically unique Si1 and Si2 sites exhibit noticeable dissimilarity [29a]. In contrast, the Ge1 and Ge2 partial DOS curves for α-$CaGe_2$ (Fig. 3) show very little difference. This is not unexpected if one recalls that Ge1 and Ge2 in the rhombohedral β-$CaGe_2$ structure form two different layers, the extent of puckering of which is very different (as exemplified by the bond distances and angles—Table 3). Nonetheless, despite these distinctive features in the anionic DOS, the theoretical considerations in both cases show some, albeit very small, covalency in the cation–anion interactions. Such partial overlap of empty states of the cations and filled states of the anions appears very little dependent on the arrangement of the polyanionic layers, making both polymorphs metallic.

4. Conclusions

A new polymorph of $CaGe_2$ has been synthesized and structurally characterized. It crystallizes in the hexagonal space group $P6_3mc$ and is closely related to the well-known rhombohedral $CaGe_2$ (isostructural with $CaSi_2$). The structure is best described as made of corrugated Ge layers interspaced by Ca cations, and the major difference between the two polymorphs is in the way these layers are arranged with respect to each other. Although the compound is nominally a Zintl phase, i.e., $Ca^{2+}(Ge_2)^{2-}$, magnetic susceptibility measurements suggest that it exhibits Pauli-like temperature independent paramagnetism, typical for materials with conducting electrons. These experimental results are reconciled with the electronic structure calculations, which confirm the existence of a conduction band arising from weak cation–anion interactions.

The studies reported herein provide another testament to the known fact that metal fluxes stabilize some intermetallic phases by carrying out reactions at lower temperatures, making it possible to isolate thermodynamically unstable phases.

Acknowledgments

Svilen Bobev acknowledges financial support from the University of Delaware through a start-up grant. Paul H. Tobash thanks the International Centre for Diffraction Data (ICDD) for the 2007 Ludo Frevel Crystallographic Fellowship.

Appendix A. Supplementary materials

Supplementary data associated with this article can be found in the online version at doi:10.1016/j.jssc.2007.03.003.

References

[1] (a) S. Sanfilippo, H. Elsinger, M. Núñez-Regueiro, O. Laborde, S. LeFloch, M. Affronte, G.L. Olcese, A. Palenzona, Phys. Rev. B 61 (2000) R3800;
(b) A.-V. Mudring, J.D. Corbett, J. Am. Chem. Soc. 126 (2004) 5277;
(c) M. Imai, T. Kikegawa, Chem. Mater. 15 (2003) 2543;
(d) T. Nakamura, T. Suemasu, K. Takakura, F. Hasegawa, A. Wakahara, M. Imai, Appl. Phys. Lett. 81 (2002) 1032;
(e) M. Imai, T. Naka, T. Furubayashi, H. Abe, T. Nakama, K. Yagasaki, Appl. Phys. Lett. 86 (2005) 032102-1;
(f) F.M. Grosche, H.Q. Yuan, W. Carrillo-Cabrera, S. Paschen, C. Langhammer, F. Kromer, G. Sparn, M. Baenitz, Yu. Grin, F. Steglich, Phys. Rev. Lett. 87 (2001) 247003-1.
[2] (a) J. Evers, J. Solid State Chem. 32 (1980) 77;
(b) H. Schäfer, K.H. Janzon, A. Weiss, Angew. Chem. Int. Ed. 2 (1963) 393.
[3] (a) G. Vogg, M.S. Brandt, M. Stutzmann, Adv. Mater. 12 (2000) 1278;
(b) K.A. Pettigrew, Q. Liu, P.P. Power, S.M. Kauzlarich, Chem. Mater. 15 (2003) 4005;
(c) G.S. Armatas, M.G. Kanatzidis, Nature 441 (2006) 1122.
[4] (a) P.H. Tobash, S. Bobev, J. Am. Chem. Soc. 128 (2006) 3532;
(b) L.-M. Wu, S. Kim, D.-K. Seo, J. Am. Chem. Soc. 127 (2005) 15682.
[5] M.G. Kanatzidis, R. Pöttgen, W. Jeitschko, Angew. Chem. Int. Ed. 44 (2005) 6996.
[6] P.H. Tobash, D. Lins, S. Bobev, A. Lima, M.F. Hundley, J.D. Thompson, J.L. Sarrao, Chem. Mater. 17 (2005) 5567.
[7] J.S. Smart, Effective Field Theories of Magnetism, Saunders, Philadelphia, PA, 1966.
[8] P. Villars, L.D. Calvert (Eds.), Pearson's Handbook of Crystallographic Data for Intermetallic Compounds, second ed., American Society for Metals, Materials Park, OH, 1991.
[9] T.B. Massalski (Ed.), Binary Alloy Phase Diagrams, American Society for Metals, Materials Park, OH, 1990.

[10] A. Palenzona, P. Manfrinetti, M.L. Fornasini, J. Alloys Compds. 345 (2002) 144.
[11] G. Vogg, M.S. Brandt, M. Stutzmann, I. Genchev, A. Bergmaier, L. Görgens, L.G. Dollinger, J. Cryst. Growth 212 (2000) 148.
[12] S. Bobev, E.D. Bauer, J.D. Thompson, J.L. Sarrao, G.J. Miller, B. Eck, R. Dronskowski, J. Solid State Chem. 177 (2004) 3545.
[13] A. Grytsiv, D. Kaczorowski, A. Leithe-Jasper, P. Rogl, M. Potel, H. Noël, A.P. Pikul, Y. Velikanova, J. Solid State Chem. 165 (2002) 178–181.
[14] Bruker SMART and SAINT, Bruker AXS Inc., Madison, WI, USA, 2002.
[15] G.M. Sheldrick, SADABS, University of Göttingen, Germany, 2003.
[16] G.M. Sheldrick, SHELXTL, University of Göttingen, Germany, 2001.
[17] The corresponding crystallographic information files (CIF) have also been deposited with Fachinformationszentrum Karlsruhe, 76344 Eggenstein-Leopoldshafen, Germany (fax: +49 7247 808 666; e-mail: crysdata@fiz.karlsruhe.de)—depository number CSD-417594 (α-$CaGe_2$) and depository number CSD-417595 (β-$CaGe_2$). Since for the first time, single crystals of $EuGe_2$ with excellent crystallographic quality became serendipitously available (above), and since the $EuGe_2$ structure had been previously established by the Rietveld method only [Ref. 12], single-crystal data collection was carried out and the structure was refined with anisotropic displacement parameters. The CIF for this refinement has a depository number CSD-417611.
[18] R.W. Tank, O. Jepsen, A. Burckhardt, O.K. Andersen, TB-LMTO-ASA Program, Version 4.7, Max-Planck-Institut Für Festkörperforschung, Stuttgart, Germany, 1998.
[19] O.K. Andersen, O. Jepsen, Phys. Rev. Lett. 53 (1984) 2571.
[20] P. Blöchl, O. Jepsen, O.K. Andersen, Phys. Rev. B 34 (1994) 16223.
[21] R. Dronskowski, P. Blöchl, J. Phys. Chem. 97 (1993) 8617.
[22] T. Hughbanks, R. Hoffmann, J. Am. Chem. Soc. 105 (1983) 3528.
[23] S.-Q. Xia, S. Bobev, Inorg. Chem. 46 (2007) 874.
[24] L. Pauling, The Nature of the Chemical Bond, third ed., Cornell University Press, Ithaca, NY, 1960.
[25] J.T. Vaughey, G.J. Miller, S. Gravelle, E.A. Leon-Escamilla, J.D. Corbett, J. Solid State Chem. 133 (1997) 501.
[26] P. Manfrinetti, M.L. Fornasini, A. Palenzona, Intermetallics 8 (2000) 223.
[27] P.H. Tobash, D. Lins, S. Bobev, N. Hur, J.D. Thompson, J.L. Sarrao, Inorg. Chem. 45 (2006) 7286 and references therein.
[28] J.R. Salvador, J.R. Gour, D. Bilc, S.D. Mahanti, M.G. Kanatzids, Inorg. Chem. 43 (2004) 1403.
[29] (a) S. Fahy, D.R. Hamann, Phys. Rev. B 41 (1990) 7587;
(b) O. Bisi, L. Braicovich, C. Carbone, I. Lindau, A. Iandelli, G.L. Olcese, A. Palenzona, Phys. Rev. B 40 (1989) 10194;
(c) S. Budnyk, F. Weitzer, C. Kubata, Y. Prots, L.G. Akselrud, W. Schnelle, K. Hiebl, R. Nesper, F.R. Wagner, Y. Grin, J. Solid State Chem. 179 (2006) 2329;
(d) F. Weitzer, Y. Prots, W. Schnelle, K. Hiebl, Y. Grin, J. Solid State Chem. 177 (2004) 2115;
(e) A. Grytsiv, D. Kaczorowski, A. Leithe-Jasper, V.H. Tran, A. Pikul, P. Rogl, M. Potel, H. Noël, M. Bohn, T. Velikanova, J. Solid State Chem. 163 (2002) 178;
(f) J. Evers, A. Weiss, Mater. Res. Bull. 9 (1974) 549;
(g) M. Affronte, O. Laborde, G.L. Olcese, A. Palenzona, J. Alloys Compds. 274 (1998) 68;
(h) Y. Imai, A. Watanabe, M. Mukaida, J. Alloys Compds. 358 (2003) 257.
[30] (a) E. Zintl, Angew. Chem. 52 (1939) 1;
(b) S.M. Kauzlarich (Ed.), Chemistry, Structure and Bonding of Zintl Phases and Ions, VCH Publishers, New York, 1996 and the references therein.